

Radio Emission from Ultra-Cool Dwarfs

P. K. G. Williams

Abstract

This is an expanded version of a chapter submitted to the Handbook of Exoplanets, eds. Hans J. Deeg and Juan Antonio Belmonte, to be published by Springer Verlag.

The 2001 discovery of radio emission from ultra-cool dwarfs (UCDs), the very low-mass stars and brown dwarfs with spectral types of \sim M7 and later, revealed that these objects can generate and dissipate powerful magnetic fields. Radio observations provide unparalleled insight into UCD magnetism: detections extend to brown dwarfs with temperatures \lesssim 1000 K, where no other observational probes are effective. The data reveal that UCDs can generate strong (kG) fields, sometimes with a stable dipolar structure; that they can produce and retain nonthermal plasmas with electron acceleration extending to MeV energies; and that they can drive auroral current systems resulting in significant atmospheric energy deposition and powerful, coherent radio bursts. Still to be understood are the underlying dynamo processes, the precise means by which particles are accelerated around these objects, the observed diversity of magnetic phenomenologies, and how all of these factors change as the mass of the central object approaches that of Jupiter. The answers to these questions are doubly important because UCDs are both potential exoplanet hosts, as in the TRAPPIST-1 system, and analogues of extrasolar giant planets themselves.

1. Introduction

The process that generates the solar magnetic field is called the *dynamo*. It is widely believed to depend on the *tachocline*, the shearing layer between the Sun's radiative inner core and its convective outer envelope (e.g., Charbonneau 2014). As stellar masses drop below \sim 0.35 M_{\odot} (spectral types \sim M3.5 and later), the tachocline disappears (Limber 1958; Chabrier & Baraffe 2000), which made it challenging to explain how mid-M dwarf stars can in fact generate strong magnetic fields (Saar & Linsky 1985).

The surprising magnetic properties of fully-convective M dwarfs raised the question of what dynamo action would be like in the coolest, lowest-mass objects: the *ultra-cool dwarfs* (UCDs), stars and brown dwarfs with spectral types M7 and later (Kirkpatrick et al. 1999; Martín et al. 1999). (The very youngest and most massive brown dwarfs have spectral types \sim M7; the very lowest-mass stars have spectral types \sim L4. Objects with spectral types between these limits can be of either category.) But it was not until the CCD revolution that it became possible to study UCDs systematically. The first results suggested that magnetic activity faded out in the UCDs (e.g., Drake et al. 1996; Basri & Marcy 1995). The consensus model was that magnetic field generation became ineffective in the lowest-mass objects due to the loss of the Sun-like “shell” dynamo and the transition to cool outer atmospheres, expected to be largely neutral and therefore unable to couple the energy of their convective motions into any fields generated below the surface (Mohanty et al. 2002). This picture was muddied, however, by reports of flares from very late M dwarfs in the ultraviolet (UV; Linsky et al. 1995), $H\alpha$ (Reid et al. 1999; Liebert et al. 1999), and X-ray (Fleming et al. 2000). These results suggested that UCDs could generate and dissipate magnetic fields at least intermittently.

A breakthrough occurred in 2001 with the detection of an X-ray flare from LP 944–20, a *bona fide* brown dwarf (M9.5; Rutledge et al. 2000), which was shortly followed by the detection of both bursting and quiescent radio emission from the same object by a team of summer students using the NRAO Very Large Array (Berger et al. 2001). Radio detections of UCDs were thought to be impossible: scaling arguments had led to radio flux density predictions of $\lesssim 0.1 \mu\text{Jy}$, not achievable even with present-day observatories. But Berger et al. (2001) detected LP 944–20 at a flux density $\sim 10^4$ times brighter than these predictions, demonstrating that UCD magnetism is — at least sometimes — vigorous and of a fundamentally different nature than observed in higher-mass objects. The detection of quiescent emission further demonstrated that not only can UCDs generate stable magnetic fields, but that they can also sustainably source the highly-energetic, nonthermal electrons needed to produce observable radio emission.

Radio observations have since proved to be the best available probe of magnetism in the UCD regime, with a major leap in capabilities coming with VLA upgrade project (Perley et al. 2011). In the rest of this chapter, we describe the phenomenology of UCD radio emission, place it in a broader astrophysical context, and deduce the implications of the data for the magnetic properties of UCDs. We close by presenting the unique contribution that studies of UCD magnetism can make to exoplanetary science and probable future directions of research in the field.

2. Phenomenology of the Radio Emission

Radio observations of UCDs have revealed a complex phenomenology that can broadly be divided into “bursting” and “non-bursting” components. The non-bursting components can also be variable and evolve significantly over long timescales (large compared to the rotation period P_{rot}) so we prefer this use this terminology rather than refer to such emission as “quiescent.” Table 1 presents the list of all known radio-active UCDs at the time of writing.

2.1. Bright, Polarized Bursts

UCDs emit bright, circularly polarized radio bursts at GHz frequencies that have durations $\tau \sim 1\text{--}100$ minutes. In the initial discovery by Berger et al. (2001), the radio bursts of LP 944–20 had a brightness temperature $T_{\text{B}} \sim 10^{10}$ K and a fractional circular polarization $f_{\text{C}} \sim 30\%$, consistent with synchrotron emission mechanisms (Dulk 1985). (Brightness temperature is a proxy for specific intensity often used by radio astronomers: $I_{\nu} \equiv 2\nu^2 k T_{\text{B}}/c^2$.) Subsequent observations have, however, revealed cases with brightness temperatures and fractional polarizations too large to be explained by synchrotron emission. In two early examples, Burgasser & Putman (2005) detected two bursts from DENIS J104814.7–395606 (M8), one with flux density $S_{\nu} \sim 20$ mJy, $\tau \sim 5$ minutes, $T_{\text{B}} \sim 10^{13}$ K, and $f_{\text{C}} \sim 100\%$. Hallinan et al. (2007) detected repeated bursts from TVLM 513–46546 (M9) with $S_{\nu} \sim 3$ mJy, $\tau \sim 5$ minutes, $T_{\text{B}} \gtrsim 10^{11}$ K, and $f_{\text{C}} \sim 100\%$ with both left- and right-handed helicities observed.

In many cases, these radio bursts have been observed to occur periodically, and in all such cases where the rotation period P_{rot} is measured through independent means,

Source name	Other name	SpT	Var?	First radio detection
2MASS J09522188–1924319 AB		M7*		McLean et al. (2012)
2MASS J13142039+1320011 B	NLTT 33370 B	M7	Y	McLean et al. (2011)
2MASS J14563831–2809473		M7		Burgasser & Putman (2005)
2MASS J00275592+2219328 AB	LP 349–25 AB	M8*	N	Phan-Bao et al. (2007)
2MASS J15010818+2250020	TVLM 513–46546	M8.5	Y	Berger (2002)
2MASS J18353790+3259545	LSR J1835+3259	M8.5	Y	Berger (2006)
2MASS J10481463–3956062	DENIS J...	M9	Y	Burgasser & Putman (2005)
2MASS J00242463–0158201	BRI B0021–0214	M9.5	Y	Berger (2002)
2MASS J03393521–3525440	LP 944–20	M9.5	Y	Berger et al. (2001)
2MASS J07200325–0846499 AB		M9.5+T5	Y	Burgasser et al. (2015)
2MASS J07464256+2000321 B		L1.5	Y	Berger et al. (2009)
2MASS J19064801+4011089	WISE J...	L1		Gizis et al. (2013)
2MASS J05233822–1403022		L2.5		Berger (2006)
2MASS J00361617+1821104		L3.5	Y	Berger (2002)
2MASS J13153094–2649513 AB		L3.5+T7		Burgasser et al. (2013)
2MASS J00043484–4044058 AB		L5+L5		Lynch et al. (2016)
2MASS J04234858–0414035	SDSS J...	L7.5	Y	Kao et al. (2016)
2MASS J10430758+2225236		L8	Y	Kao et al. (2016)
2MASS J06073908+2429574	WISE J...	L9		Gizis et al. (2016)
2MASS J01365662+0933473	SIMP J...	T2.5	Y	Kao et al. (2016)
WISEP J112254.73+255021.5		T6	Y	Route & Wolszczan (2016)
2MASS J10475385+2124234		T6.5	Y	Route & Wolszczan (2012)
2MASS J12373919+6526148		T6.5	Y	Kao et al. (2016)

Table 1: The twenty-three radio-detected UCDs as of mid-2017. “SpT” shows a spectral type from SIMBAD; UCD spectral typing is challenging and subtle (e.g., Kirkpatrick et al. 2012), but to conserve space we omit details and references. Spectral types with asterisks (*) are known to come from the blended spectra of more than one object. “Var?” indicates whether the source has been confirmed to have radio emission that varies on short ($\lesssim 1$ hr) time scales. This is the case for all well-studied UCDs except LP 349–25 AB (Osten et al. 2009).

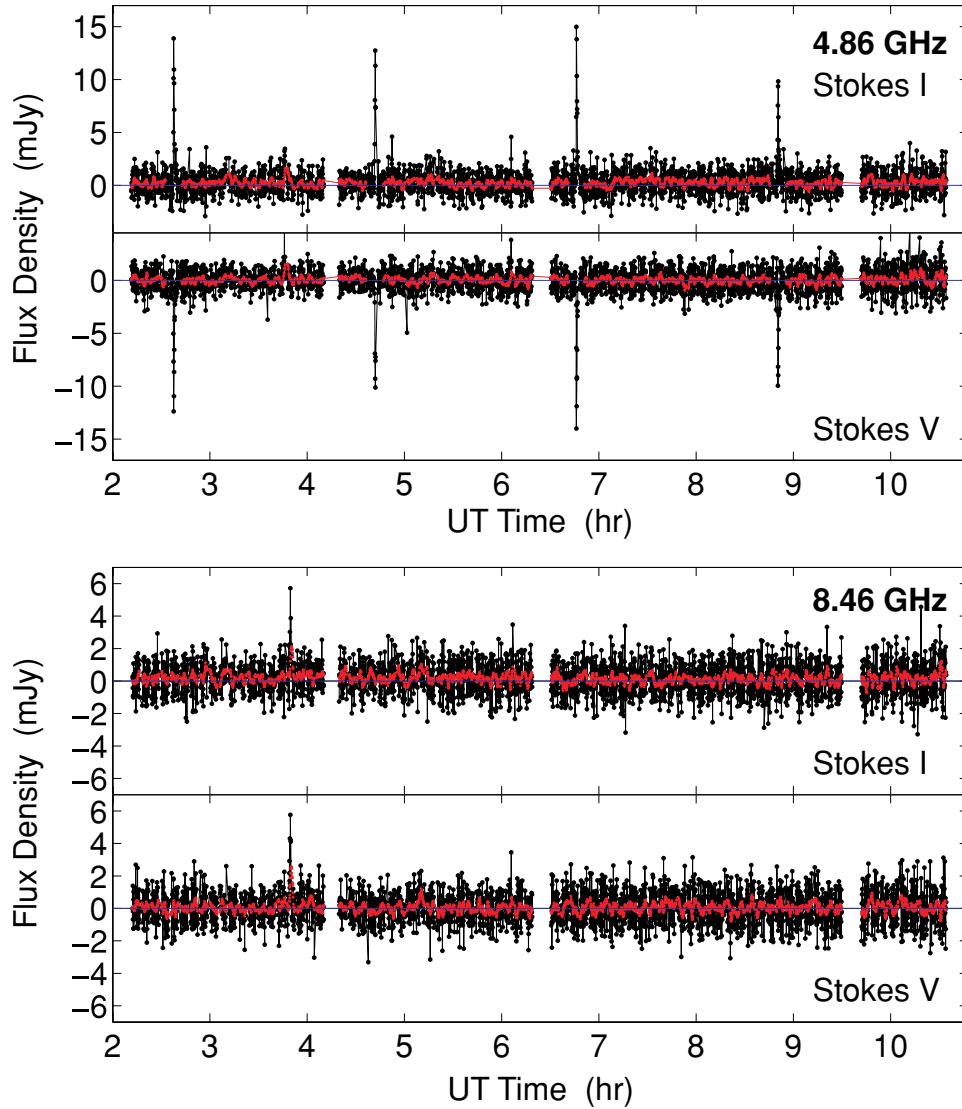


Figure 1: [From Berger et al. (2009). Reproduced by permission of the AAS.] Radio light curve of 2MASS J07464256+2000321 B showing periodic, highly polarized, rapid, bright bursts. The black and red points show the data averaged into 5- and 60-second bins, respectively. The negative Stokes V values, $|V| \sim I$, indicate $\sim 100\%$ left circular polarization in the bursts. The burst spectra do not extend to the VLA’s 8.46 GHz band (lower panels).

the periodicity of the bursts matches P_{rot} . [Figure 1](#) shows a classic example of this phenomenology from [Berger et al. \(2009\)](#). In the objects with such measurements, $2 \lesssim P_{\text{rot}} \lesssim 4$ h, but there are likely significant selection effects at play that make it difficult to infer the true distribution of P_{rot} of the radio-active UCDs. In objects with repeated observations, the periodic bursts are sometimes present and sometimes not (e.g., LSR J1835+3259; [Berger et al. 2008a](#); [Hallinan et al. 2008](#)). TVLM 513–46546 is the best-studied member of this class, with burst observations spanning years that enable claims of extremely precise (millisecond) determinations of the rotation period ([Doyle et al. 2010](#); [Harding et al. 2013a](#); [Wolszczan & Route 2014](#)).

These bursts have been generally been detected at frequencies between 1 and 10 GHz. Once again, selection effects make it difficult to draw conclusions about the fundamental character of the burst spectra given the observational results: the vast majority of searches for UCD radio emission of have been conducted in the 1–10 GHz frequency window. This window is where the VLA’s sensitivity peaks, but it is challenging to quantify how important intrinsic effects are as well (we observe in this window because there truly are more bursts to be seen in it). The spectral shapes of the bursts are not fully understood. Both high- and low-frequency cutoffs have been observed in different bursts ([Lynch et al. 2015](#); [Williams et al. 2015a](#)), but in no burst has there been definitive evidence that the flux density peak has been identified. Later in this chapter we will argue that the bursts are probably of moderate bandwidth, $\Delta\nu/\nu \sim 1$.

The total energy contained in the bursts is not large, which is commonly the case for radio processes. Using the properties of the bursts from TVLM 513–46546 quoted above ([Hallinan et al. 2007](#)), the energy content of an individual burst is $\sim 10^{27}$ erg, assuming isotropic emission. For coherent emission processes the emission is unlikely to be isotropic, reducing the energy budget further. The burst luminosities are typically $\approx 10^{-6}$ of the bolometric (sub)stellar radiative output.

2.2. Non-bursting Emission

UCDs also produce non-bursting radio emission that is generally steady over the time scales of individual observations. Repeated observations of numerous UCDs have revealed, however, that this emission often varies at the order-of-magnitude level on longer (\sim week and above) timescales (e.g., [Antonova et al. 2007](#); [McLean et al. 2012](#)). Several UCDs have been detected once in the radio and not detected in deeper follow-up observations (e.g., [McLean et al. 2012](#)). On the other hand, archival detections show that the hyperactive M7 star NLTT 33370 B has sustained a broadly consistent level of radio emission for at least a decade ([McLean et al. 2011](#)). [Figure 2](#) shows that this object, the most radio-bright UCD, nonetheless displays both periodic (at P_{rot}) and long-term variability in its radio emission.

Radio-detected UCDs typically have non-bursting spectral luminosities of $L_{\nu, \text{R}} \sim 10^{12}\text{--}10^{14}$ erg s $^{-1}$ Hz $^{-1}$, usually about an order of magnitude fainter than the peak observed burst luminosity when both phenomena have been observed. Selection effects are important here, too: the lower bound of this range corresponds to the sensitivity that is achieved in typical VLA reconnaissance observations (~ 1 hr duration) of nearby (~ 10 pc) UCDs. The deepest upper limit on a UCD is $\sim 10^{11}$ erg s $^{-1}$ Hz $^{-1}$, obtained in observations of the nearby binary Luhman 16 AB ([Osten et al. 2015](#)). The brightest

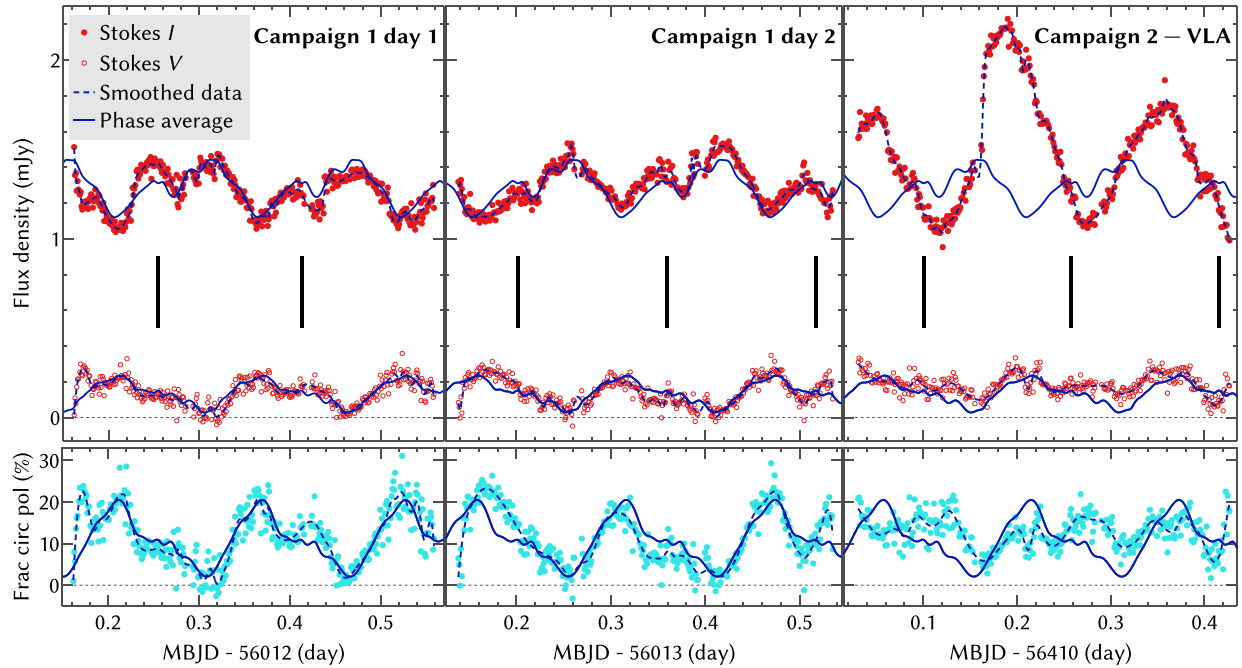


Figure 2: [From Williams et al. (2015a). Reproduced by permission of the AAS.] Radio light curve of NLTT 33370 B showing periodic variation and moderate polarization in the non-bursting radio emission. In the upper panels, filled and empty points show Stokes I and V components, respectively. The lower panels show the fractional circular polarization derived from these values. The leftmost and center panel show two observations separated by 24 hr; the rightmost panel shows observations made ~ 1 yr later. Vertical black lines indicate times that the dwarf’s periodically-modulated optical emission reaches maximum. Rapid, 100% circular polarized radio bursts have been excised from these data.

UCD radio emitter, NLTT 33370 B, reaches $\sim 10^{14.7}$ erg s $^{-1}$ Hz $^{-1}$ (McLean et al. 2011; Williams et al. 2014).

The non-bursting emissions generally have low or moderate circular polarization. Linear polarization has not been detected. As shown in Figure 2, $0 < f_C < 20\%$ in the case of NLTT 33370 B, with periodic variability at P_{rot} indicating that the apparent circular polarization depends on orientation. The recently discovered radio-active T6.5 dwarf WISEP J112254.73+255021.5 presents a new, unusual case: unlike the other UCDs, WISEP J112254.73+255021.5 produces highly polarized emission that is not clearly confined to rapid bursts (Williams et al. 2017). The only published observations of this object are too brief, however, to allow a firm interpretation.

The non-bursting spectra are broadband. They peak around 1–10 GHz and generally have shallow spectral indices on both the low- and high-frequency sides of the peak. Only a few UCDs have been observed at a wide range of radio frequencies, however. TVLM 513–46546 has been detected at frequencies ranging from 1.4 GHz all the way to 98 GHz; the latter detection was achieved with ALMA and represents the first demonstration that UCDs can be detected at millimeter wavelengths (Williams et al. 2015b). NLTT 33370 B has been detected from 1–40 GHz (McLean et al. 2011; Williams et al. 2015a) and has an extremely flat spectrum, with significant circular polarization at all observed frequencies. DENIS J104814.7–395606 has been detected from 5–18 GHz with a negative spectral index $\alpha = -1.71 \pm 0.09$ ($S_\nu \propto \nu^\alpha$; Ravi et al. 2011). Searches for emission from UCDs at frequencies below 1 GHz have thus far been unsuccessful (Jaeger et al. 2011; Burningham et al. 2016) although the famous low-mass flare star UV Cet (M6) was recently detected at 154 MHz using the Murchison Widefield Array (Lynch et al. 2017).

2.3. Intermediate Cases

It is not always possible to cleanly separate UCD radio emission into bursting and non-bursting components. Figure 3 shows an example from TVLM 513–46546 in which variability is observed with both circular polarization helicities as well as null polarization (Hallinan et al. 2006). 2MASS J00361617+1821104 and NLTT 33370 B have shown similarly ambiguous phenomenologies (Berger et al. 2005; Hallinan et al. 2008; Williams et al. 2015a).

3. UCD Radio Emission in Context

The previous section focused narrowly on the properties of the radio emission detected from UCDs. In this section, we place this emission in a broader astrophysical context.

3.1. The Prevalence of Radio Activity in UCDs

Volume-limited radio surveys of UCDs achieve a detection rate of approximately 10% (Berger 2006; McLean et al. 2012; Antonova et al. 2013; Lynch et al. 2016). However, recent work by Kao et al. (2016) demonstrates that biased surveys can achieve a substantially higher detection rate: in a sample of five late-L and T dwarfs selected to have prior detections of H α emission or optical variability, four of the targets were detected.

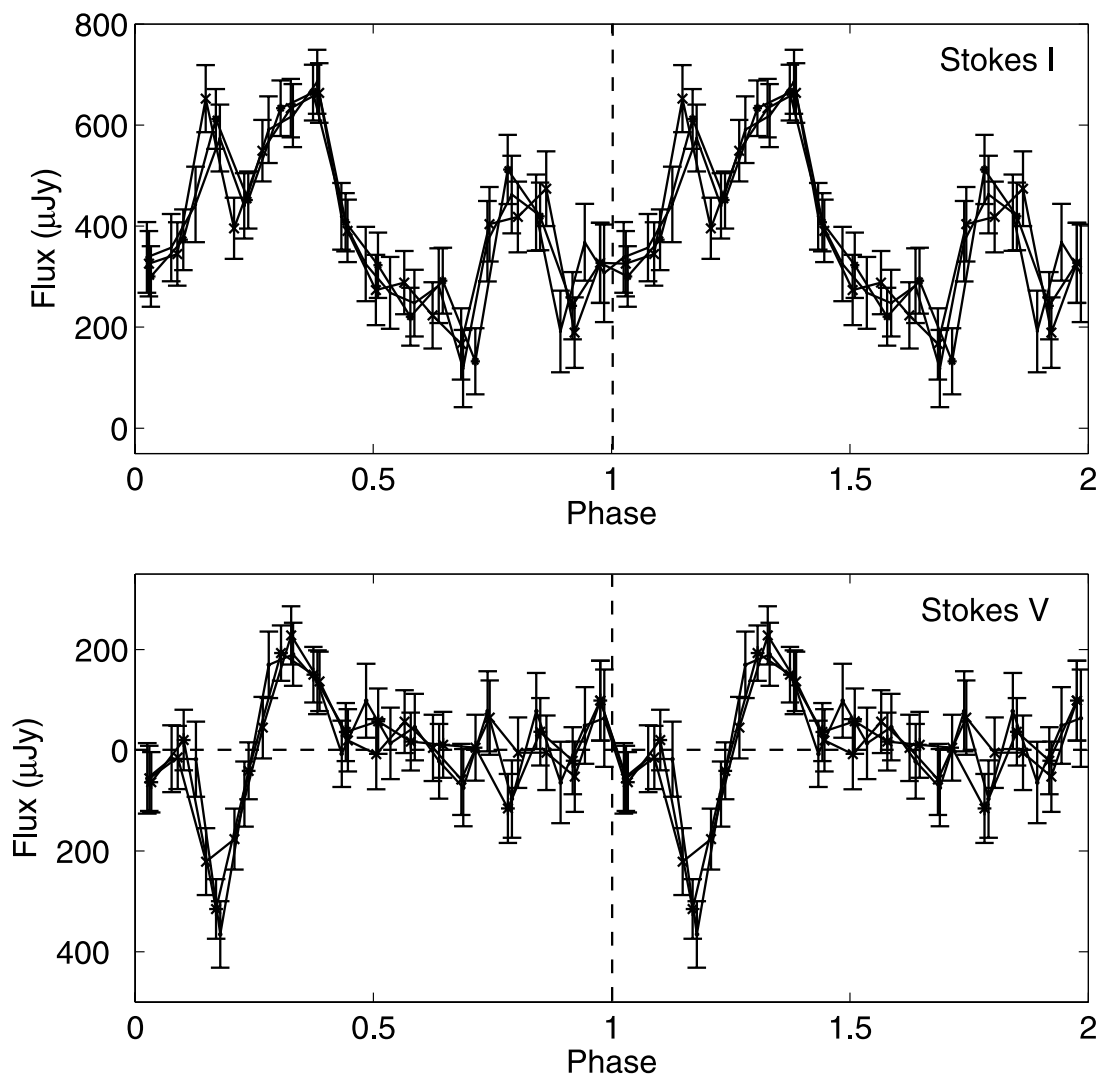


Figure 3: [From Hallinan et al. (2006). Reproduced by permission of the AAS.] Radio light curve of TVLM 513–46546 showing periodic behavior that is not cleanly separable into burst and non-burst components. The data are phased to a period of 2 hr and shown binned at 6, 7, and 8 minutes, with each binned light curve being plotted twice. The observing frequency was 4.88 GHz.

These findings are consistent because the $H\alpha$ detection rate of L and T dwarfs is also about 10% on average, with a noticeably higher detection rate for objects warmer than $\sim L5$ (Pineda et al. 2016).

This “headline number” comes with three important caveats. First, it derives from an observer-dependent binary classification (“did the object’s apparent radio flux density have sufficiently high S/N?”) rather than a fundamental physical measurement (“what is the object’s radio spectral luminosity?”). Second, the radio detectability of individual objects varies over time in ways that are not well understood. Third, the reported number averages across a wide variety of objects, while studies of FGKM dwarfs lead us to expect that activity strength should depend strongly on fundamental (sub)stellar parameters.

In particular, mass, rotation, and age are generally believed to be the most important for setting stellar activity levels (e.g., Barnes 2003; Wright et al. 2011). Correlations between fundamental parameters are pervasive, however, so it is challenging to determine causation (e.g., Reiners et al. 2014). Below we consider how UCD radio emission scales with some of these physical parameters, *considering only the radio-detected objects*. A proper analysis of the entire radio-observed UCD sample that takes into account nondetections has yet to be performed. Numerous UCDs have upper limits on their radio emission that are inconsistent with the trends described.

3.1.1. Mass, Spectral Type, and Effective Temperature

Because brown dwarfs do not evolve to a stable main sequence and direct mass measurements of astronomical objects are difficult to obtain, spectral type (SpT) is widely used as a proxy for mass in UCD activity studies.

The magnetic activity levels of FGKM stars are often quantified with the ratio of the stellar X-ray luminosity to bolometric luminosity (L_X/L_{bol} ; e.g., Wright et al. 2011). This ratio decreases as SpT increases (that is, moves toward cooler T_{eff}) even though L_{bol} on its own scales strongly with T_{eff} , implying a significant drop in the un-normalized L_X (Stelzer et al. 2006; Berger et al. 2010; Williams et al. 2014). It is therefore striking that in UCDs, $L_{\nu,R}$ shows only a mild decrease with SpT, with typical values of $\sim 10^{13.5} \text{ erg s}^{-1} \text{ Hz}^{-1}$ at M7 and $\sim 10^{12.5} \text{ erg s}^{-1} \text{ Hz}^{-1}$ in the T dwarfs (Gizis et al. 2016, their Figure 8). Over this range of SpTs $L_{\nu,R}/L_{\text{bol}}$ increases from typical values of $\sim 10^{-17} \text{ Hz}^{-1}$ to $\sim 10^{-16} \text{ Hz}^{-1}$.

3.1.2. Rotation

Magnetically active FGKM stars follow a “rotation/activity relation” in which the level of magnetic activity increases with increasing rotation rate up until a “saturation point,” past which further increases in rotation rate do not affect the level of magnetic activity (e.g., Wright et al. 2011). Here the level of magnetic activity is most commonly quantified with L_X/L_{bol} , but analogous trends are observed in most other measurements that trace activity.

The nature of the radio rotation/activity relationship in UCDs is more ambiguous. Plots of $L_{\nu,R}/L_{\text{bol}}$ against rotation show a scaling relationship that has no sign of a saturation point (McLean et al. 2012). However, the fastest rotators tend to be the objects with the latest spectral types, introducing a covariance with the mass trend described above. Cook et al. (2014) studied a subset of UCDs at a relatively

narrow range of SpT, M6.5–M9.5, and found weak evidence that L_X/L_{bol} is in fact *anti*-correlated with rotation rate.

3.1.3. Age

Sun-like stars become less active as they age since they shed angular momentum through their winds (Skumanich 1972). This process becomes much less efficient as stellar mass decreases, with the average activity lifetime of M dwarfs going from ~ 1 Gyr for M0–M2 stars to ~ 8 Gyr for M5–M7 stars (West et al. 2008). The data suggest that brown dwarfs rotate rapidly for their entire lives (Bouvier et al. 2014).

The relation between age and radio activity has not been studied systematically in UCDs. However, several noteworthy radio-active UCDs have age constraints, including LP 944–20 (~ 500 Myr; Tinney & Reid 1998), NLTT 33370 B (~ 80 Myr; Dupuy et al. 2016), and SIMP J01365662+0933473 (~ 200 Myr; Gagné et al. 2017). Very young UCDs can also have radio emission associated with young-star phenomena such as accretion, jets, and disks (e.g., Rodriguez et al. 2017).

3.2. Multi-wavelength Correlations

Stellar magnetism is associated with emission across the electromagnetic spectrum, and different bands probe different physical regions or processes. In Sun-like stars, H α emission probes the chromosphere; UV, the transition region; X-rays, hot dense coronal plasma; and radio/millimeter emission, particle acceleration. Multi-wavelength observations, especially simultaneous ones, therefore yield insights that cannot be obtained through single-band studies.

The radio and X-ray luminosities of active stars are nearly linearly correlated, a phenomenon known as the “Güdel-Benz relation” (Güdel & Benz 1993; Benz & Güdel 1994). A single power law can fit observations spanning ten orders of magnitude in $L_{\nu, R}$, in systems ranging in size from individual solar flares to active binaries (Figure 4, gray points). As shown above, however, the Güdel-Benz relation breaks down dramatically in the UCD regime (Figure 4, colored points; Berger et al. 2001; Williams et al. 2014). Correlations between the luminosities of UCDs in radio and other bands (e.g., H α) have not yet been investigated in the literature.

Simultaneous multi-wavelength observations can illuminate the physics of stellar and substellar flares, although extensive observations of flare stars demonstrate that very few general statements can be made: individual events may or may not be associated with emission in each of the bands that trace magnetic activity, and the relative ordering and magnitude of the emission in these bands is variable (e.g., Osten et al. 2004). The UCD with the best simultaneous multi-wavelength observational coverage is NLTT 33370 B, and the data show a similar variety of phenomenologies (Williams et al. 2015a). A detailed understanding of the underlying physics remains elusive.

The evidence that optical/IR variability is a useful indicator of UCD radio activity (Kao et al. 2016) suggests that the two are correlated. Only a handful of UCDs have data sets that allow the optical and radio variability (either bursts or non-bursting periodic variations) to be phased. While the radio and optical maxima of TVLM 513–46546 are significantly out of phase (Wolszczan & Route 2014; Miles-Páez et al. 2015), there is a hint that the millimeter and optical maxima may occur at the same phase (Williams et al. 2015b). The radio and optical maxima of NLTT 33370 B are also significantly

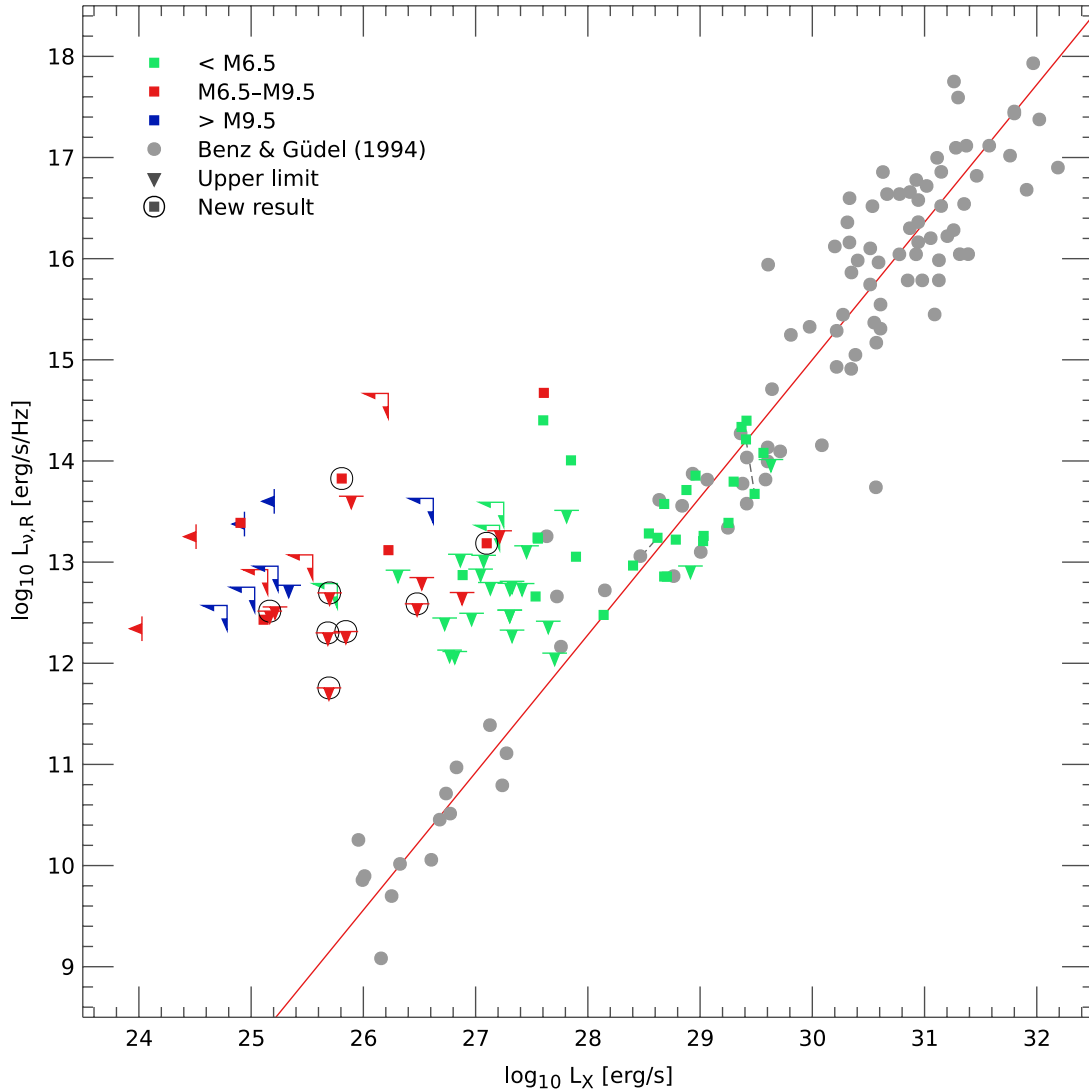


Figure 4: [From Williams et al. (2014). Reproduced by permission of the AAS.] Radio and X-ray emission for active stars and brown dwarfs. Gray points and the red line show the “Güdel-Benz relation” defined for active stars and solar flares. Green, red, and blue points show data for M3–M6, M6.5–M9.5, and $\geq L0$ dwarfs, respectively. While some UCDs may obey the Güdel-Benz relation, there is a substantial population of outliers with radio emission that far exceeds what would be predicted from their X-ray emission.

out of phase. Intriguingly, long-term monitoring of this object suggests that its non-bursting polarized radio emission remains in phase with its optical variability but the total radio intensity does not (Williams et al. 2015a). *Keck* spectroscopic monitoring of LSR J1835+3259 revealed periodic variations in the optical emission that were argued to originate in a high-altitude opaque blackbody with $T \sim 2200$ K (Hallinan et al. 2015).

Radio and H α variability can also be correlated. In 2MASS J07464256+2000321 B, the radio bursts are 90° out of phase with the maxima of periodic changes in the H α equivalent width (Berger et al. 2009). Recent observations of LSR J1835+3259 showed radio and H α variations that were approximately in phase (Hallinan et al. 2015), but other observations of the same object have shown aperiodic H α variability with no clear connection to the radio emission (Berger et al. 2008a). Simultaneous multi-wavelength monitoring of TVLM 513–46546 revealed periodic H α variability with no clear connection to emission in other bands, although there is some evidence for radio bursts at the times of the H α minima (Berger et al. 2008b).

4. Interpretation of the Data

We now turn to the astrophysical interpretation of the observations presented in the previous sections.

4.1. Auroral Radio Emission

The periodic, bright, highly-polarized radio bursts observed in radio-active UCDs are consistent with the auroral radio bursts observed in Solar System planets (Zarka et al. 2001), which are generally agreed to originate from the electron cyclotron maser instability (ECMI; Wu & Lee 1979; Treumann 2006). The ECMI converts the free energy of a magnetized plasma into electromagnetic waves through resonant interactions between the waves and the particles' cyclotron motion. The ECMI is relatively easy to trigger in physical systems involving beams of mildly relativistic electrons that are accelerated along magnetic field lines by the presence of a co-aligned electric field, if the ambient medium is of sufficiently low density. This happens at the Earth when energetic solar wind particles funnel down its magnetic field lines toward the poles.

Observable ECMI emission is expected to be dominated by a narrow-band signal at the electron cyclotron frequency of the local magnetic field,

$$\nu_{ce} = \frac{eB}{2\pi m_e c} \sim 2.8 \left(\frac{B}{1 \text{ G}} \right) \text{ MHz.} \quad (1)$$

Observations of ECMI bursts from UCDs therefore measure the strengths of their magnetic fields. In practice, the ECMI occurs in regions that span a variety of field strengths, so the observed emission has a moderate bandwidth, $\Delta\nu/\nu \sim 1$ (Zarka et al. 2001), with a cutoff at high frequencies because the body's magnetic field reaches some peak value at its surface. ECMI emission is beamed and likely refracts through the plasmasphere that evidently envelops the radio-active UCDs, necessitating detailed simulations to predict its observed properties (e.g., Kuznetsov et al. 2012; Yu et al. 2012).

At a typical VLA observing frequency of ~ 5 GHz, the inferred strength is ~ 2 kG, comparable to the strongest surface field strengths observed on active M dwarfs (Kochukhov et al. 2017). A polarized pulse at 10 GHz from the T6.5 dwarf 2MASS J10475385+2124234 implies a field strength of at least 3.6 kG (Williams & Berger 2015), demonstrating that the fully convective dynamo can generate strong fields even in extremely low-mass, cool (~ 900 K) objects.

Observations of multiple consecutive ECMI bursts at the rotation period imply the presence of a relatively stable “electrodynamical engine” that accelerates the beams of electrons responsible for the emission. Understanding the nature of this engine is one of the great tasks in the field of UCD magnetism. In the Solar System planets, the engine is often powered by the solar wind (e.g., Dungey 1961; Axford 1969), but this driver is not available for solivagant UCDs. The only persuasive explanation is that the engine is ultimately powered by the body’s rotation (Schrijver 2009). This is largely the case for Jupiter (McComas & Bagenal 2007), raising the exciting possibility that sophisticated models developed in the context of the Solar System gas giants can be brought to bear on the UCD case. For instance, studies of Jupiter inform a model in which rotational energy is converted into nonthermal particle acceleration through shear-induced currents at the corotation breakdown radius (Nichols et al. 2012).

Rapid rotation and the stable operation of the electrodynamic engine imply that the magnetospheres of radio-active UCDs likely have dipole-dominated topologies. This inference is supported by observations that probe the topologies of the magnetic fields of cool stars. Studies using Zeeman Doppler Imaging (ZDI; Semel 1989) show that strong, axisymmetric, dipolar fields emerge in the coolest M dwarfs currently accessible to the technique (Morin et al. 2010) and that such a topology may be associated with enhanced radio activity and variability (Kochukhov & Lavail 2017).

Auroral electron beams do not only produce radio emission. First, auroral processes are associated with emission across the electromagnetic spectrum, with the highest luminosities concentrated at FUV and IR wavelengths (Bhardwaj & Gladstone 2000). However, the emission at these wavelengths is not nearly as bright as it is in the radio, such that the auroral fluxes in other bands inferred for known active UCDs are beyond the capabilities of present-day instruments. Second, the energetic auroral electrons eventually precipitate into the upper atmosphere, where they can drive chemical processes like haze production (e.g., Wong et al. 2003). Hallinan et al. (2015) interpreted their simultaneous radio and optical observations in this framework, arguing that an electron beam delivering 10^{24} – 10^{26} erg s^{-1} of kinetic power drove both the radio emission of LSR J1835+3259 and its optical variability by creating a compact, high-altitude layer of H^- upon precipitation. This model also motivated the targeted survey of Kao et al. (2016), under the assumption that auroral electron beams cause detectable $H\alpha$ and/or optical variability. A recent study, however, does not find a correlation between $H\alpha$ and high-amplitude optical variability in a large sample of L/T dwarfs (Miles-Páez et al. 2017).

4.2. Gyrosynchrotron Radio Emission

Non-bursting UCD radio emission bears the hallmarks of gyrosynchrotron emission, the same process that is believed to be responsible for the bulk of the radio emission observed from active stars (Dulk 1985; Güdel 2002). Gyrosynchrotron emission is pro-

duced by mildly relativistic electrons spiraling in an ambient magnetic field, resulting in a broadband spectrum with low to moderate circular polarization. Analysis of the spectral properties can constrain the ambient magnetic field strength, the total number and volume density of energetic particles, and their energy distribution. It has been argued that the non-bursting UCD radio emission may instead represent an unusual form of ECMI emission (Hallinan et al. 2006, 2008), but several lines of evidence, most notably the millimeter-wavelength detection of TVLM 513–46546, discourage this interpretation (Williams et al. 2015a,b).

The standard equations for gyrosynchrotron emission are derived for spatially homogeneous field and particle properties (Dulk 1985). A robust result of this analysis is that the optically-thick (low-frequency) side of the spectrum should have a spectral index $\alpha = 5/2$, much steeper than that observed for sources like NLTT 33370 B and TVLM 513–46546 (Osten et al. 2006; McLean et al. 2011). While the flat observed spectra can be reproduced qualitatively with more realistic inhomogeneous models (e.g., White et al. 1989; Trigilio et al. 2004), homogeneous models should still give a sense of the average properties of the emitting region. Spectral fits with both kinds of model suggest that the ambient field strength in the synchrotron-emitting region is $\sim 10\text{--}100$ G, typical of flare stars (Berger 2006; Osten et al. 2006; Metodieva et al. 2017). Assuming standard energetic electron densities and brightness temperatures, the typical source size is a few R_* (Berger 2006; Williams et al. 2014). The fact that R_* evolves only slowly with mass in the UCD regime may help explain why $L_{\nu,R}$ appears to settle at a typical value of $\sim 10^{13}$ erg s $^{-1}$ Hz $^{-1}$ in the radio-active UCDs, if the other factors that set the synchrotron radio luminosity (B and n_e) are also mass-insensitive. Radio emission is energetically insignificant, so if the particle acceleration process saturates in some way, this value of $L_{\nu,R}$ could be achieved in UCDs with widely varying bolometric and spindown luminosities.

Analyses of the non-bursting radio emission of UCDs have not yet begun to leverage the detailed models that have been developed for analogous systems. Magnetic chemically peculiar (MCP) stars have high masses but also possess strong, dipole-dominated magnetospheres with persistent and periodically variable radio emission. Numerical modeling of MCP particle populations can constrain the magnetospheric structure in detail (Trigilio et al. 2004; Leto et al. 2017). Even more excitingly, Jupiter’s radiation (van Allen) belts have been studied in exquisite detail and produce centimeter-wavelength emission with variability, spectra, and polarization that are highly reminiscent of the UCD observations (de Pater 1981; de Pater et al. 2003). The application of Jovian models to UCD data has the potential to yield a treasure trove of insight. For instance, the presence of Jupiter’s moons can be inferred from the spectrum of its radiation belts alone (Santos-Costa & Bolton 2008), and observations made at different orientations of the planet can be combined to reconstruct the full three-dimensional structure of the belts (Sault et al. 1997).

4.3. The Emergence of “Planet-like” Magnetism in UCDs

The data show that UCDs can generate strong magnetic fields and dissipate their energy vigorously, but that they do so in processes that are fundamentally different than the typical flare star phenomenology. This is demonstrated most clearly by the substantial drop in UCD X-ray emission (both L_X and L_X/L_{bol}), violation of the Güdel-

Benz relation, and the emergence of periodic, bright, highly-polarized radio bursts.

This can be understood as the emergence of “planet-like” magnetism in UCDs, characterized by processes that occur in large-scale, stable, rotation-dominated magnetospheres (Schrijver 2009). These include the operation of an electrodynamic engine that accelerates auroral electron beams and sustains a population of mildly relativistic electrons. The lack of X-ray emission indicates that coronal heating, if it can be said to occur at all, does not happen in a Sun-like fashion. Historically, this has been explained as being due to the outer atmosphere becoming electrically neutral and therefore unable to couple the energy of convective motions into magnetic flux tubes (Mohanty et al. 2002). More recent work has argued that UCD atmospheres should in fact still couple to the magnetic field efficiently (Rodríguez-Barrera et al. 2015), suggesting that more detailed analysis is needed.

One of the fundamental questions about this picture is why only $\sim 10\%$ of UCDs are detected in the radio. While early thinking focused on the possible roles of inclination and rotation rate (e.g., Harding et al. 2013b), current data suggest that planet-like magnetism is only *sometimes* present in UCDs and that the presence or absence of planet-like behavior is not linked to any particular fundamental parameter. The most compelling evidence for this is the NLTT 33370 AB system: while NLTT 33370 B is the most radio-luminous UCD known, its binary companion is at least 30 times fainter than it, despite being nearly identical in mass, age, rotation rate, and composition (Williams et al. 2015a; Dupuy et al. 2016; Forbrich et al. 2016). Population studies show evidence for bimodality when considering the Güdel-Benz relation (Stelzer et al. 2012; Williams et al. 2014), the rotation/activity relation (Cook et al. 2014), and ZDI-derived magnetic field topologies (Morin et al. 2010).

The large-scale topology of the magnetic field may be the key factor that determines whether planet-like magnetic behavior arises in a given UCD (Cook et al. 2014). This hypothesis is tenable because geodynamo simulations indicate that the fully convective dynamo may be bistable in the conditions encountered in the UCD regime, with identical objects sustaining different topologies depending on initial conditions (Gastine et al. 2013). Recent observations provide the first direct evidence for this model: ZDI reveals that UV Cet ($\sim M6$) has an axisymmetric, dipole-dominated magnetic field, while the field of its nearly-identical binary companion BL Cet is weaker and non-axisymmetric (Kochukhov & Lavail 2017). Consistent with the proposed model, UV Cet is more luminous and variable in the radio than BL Cet.

Detectable radio emission requires the presence of both a magnetic field *and* non-thermal electrons. The difference between the radio-active and -inactive UCDs may therefore hinge not on the field topology but on the presence of a source of plasma that can eventually produce the gyrosynchrotron and ECMI emission. In analogy with Jupiter, the 10% of UCDs that are radio-active might be the ones possessing volcanic planets resembling Io. This scenario can potentially be tested by searching for ECMI bursts that repeat periodically not at P_{rot} but at the synodic period of the planetary orbit. No evidence of such a non-rotational periodicity has yet been reported.

5. The Exoplanetary Connection

Radio studies of UCDs make a unique contribution to exoplanetary science because they are the only effective way to observe the magnetic properties of cool, extrasolar

bodies.

One reason that this is important is that UCDs may host large numbers of observationally-accessible small planets, as demonstrated by the TRAPPIST-1 system (Gillon et al. 2016, 2017). Understanding UCD activity is therefore important for the same reasons that it is important for any exoplanet host star: magnetic phenomena make planet discovery more challenging (e.g., Robertson et al. 2014) and they can have a significant impact on atmospheric retention and the broader question of habitability (e.g., Jakosky et al. 2015; Shields et al. 2016). Because UCD magnetism can be so different from that of Sun-like stars and M dwarfs, its impact on habitability may differ substantially from the cases that have been investigated thus far in the literature. For instance, the detection of millimeter-wavelength radiation from TVLM 513–46546 points to a surprisingly high-energy radiation environment of MeV electrons, which can produce γ -ray emission when they precipitate into the stellar atmosphere (Williams et al. 2015b). The moons of the Solar System gas giants should serve as useful reference points in this domain (e.g., Paty et al. 2008).

UCD magnetic fields can strongly resemble those of the Solar System gas giant planets. Radio observations therefore provide insight into the magnetospheres of exoplanets themselves, which observers have been struggling to probe since well before the first confirmed exoplanet discovery (Yantis et al. 1977). Currently, exoplanetary magnetospheres can only be investigated using indirect and model-dependent means (e.g., Ekenbäck et al. 2010). Direct observations of exoplanetary magnetospheres would not only shed light on the question of habitability, but also internal structure; for instance, magnetic field generation in rocky planets may require the presence of plate tectonics (Breuer et al. 2010). The first direct measurement of the magnetic field of a planetary-mass object may already have occurred, because SIMP J01365662+0933473, detected in the radio by Kao et al. (2016), was recently argued to be a member of the ~ 200 -Myr-old Carina-Near moving group, which would give it a mass of 12.7 ± 1.0 M_J according to standard evolutionary models (Gagné et al. 2017).

6. Future Directions of Research

One of the top priorities in the field of UCD radio studies is the extension of its techniques to genuine exoplanets. By analogy with Solar System examples, exoplanets are expected to have magnetic fields that are much weaker than those of UCDs, which leads to the expectation that their radio emission will occur at lower radio frequencies, $\lesssim 300$ MHz. Fortunately the past decade has witnessed a dramatic investment in low-frequency radio arrays such as the Low Frequency Array (LOFAR), the Murchison Widefield Array (MWA), the Long-Wavelength Array (LWA), the Giant Metrewave Radio Telescope (GMRT), and the Hydrogen Epoch of Reionization Array (HERA). While the first generation of these instruments has not yielded any detections of genuine UCDs, the first positive results are starting to emerge (Lynch et al. 2017), and virtually all of these observatories are undergoing upgrades that are expected to yield significant sensitivity improvements.

While many of the nearest UCDs have been surveyed by the Very Large Array, the results of Kao et al. (2016) suggest that targeted searches may be able to yield detections beyond the typical detection horizon (~ 30 pc) for blind searches thus far. Furthermore, radio studies of southern UCDs have historically been hampered by the

lack of an instrument as powerful as the VLA (latitude $+34^\circ$). The commissioning of the MeerKAT radio telescope in South Africa (Jonas 2009), with science operations slated to begin in late 2017, will introduce a powerful new observatory in the south. MeerKAT should be especially valuable in surveys for radio emission from young, directly-imaged exoplanets, which are promising targets because they are as warm, or even warmer, than the coolest UCDs with confirmed radio detections, and convect vigorously. Most of the currently-known young planets are in the southern hemisphere, however, and have not been the subject of sensitive radio observations. Surveys for radio-active UCDs in both hemispheres will be transformed by the deeper insight into the natures of the stars and brown dwarfs in the solar neighborhood afforded by upcoming surveys from observatories such as Gaia, the Transiting Exoplanet Survey Satellite (TESS), and Spektr-RG, the spacecraft bearing the e-ROSITA instrument.

Finally, a great deal of theoretical work remains to be done. More detailed models of the bursting and non-bursting radio emission will strengthen the astrophysical inferences that can be drawn from the radio data. The populations statistics of radio-active UCDs should be understood better by a more rigorous treatment of the many nondetections and a more careful characterization of the long-term variability of their radio emission. This sort of work will lay the foundations upon which models can be constructed that explain fundamental puzzles such as the source of the radio-emitting plasma, the possible existence of a bistable dynamo, and the relationship between rotation and magnetic activity in the ultra-cool regime.

Acknowledgments. P.K.G.W. thanks Edo Berger for supporting his work in this field and Adam Burgasser, Kelle Cruz, Trent Dupuy, Jackie Faherty, Gregg Hallinan, Mark Marley, and Rachel Osten for many enlightening conversations over the years. P.K.G.W. acknowledges support for this work from the National Science Foundation through Grant AST-1614770. This research has made use of the SIMBAD database, operated at CDS, Strasbourg, France and NASA’s Astrophysics Data System.

References

- Antonova, A., Doyle, J. G., Hallinan, G., Golden, A., & Koen, C. 2007, *A&A*, 472, 257
 Antonova, A., Hallinan, G., Doyle, J. G., et al. 2013, *A&A*, 549, A131
 Axford, W. I. 1969, *Review of Geophysics and Space Physics*, 7, 421
 Barnes, S. A. 2003, *ApJ*, 586, 464
 Basri, G., & Marcy, G. W. 1995, *AJ*, 109, 762
 Benz, A. O., & Güdel, M. 1994, *A&A*, 285, 621
 Berger, E. 2002, *ApJ*, 572, 503
 —. 2006, *ApJ*, 648, 629
 Berger, E., Ball, S., Becker, K. M., et al. 2001, *Natur*, 410, 338
 Berger, E., Rutledge, R. E., Reid, I. N., et al. 2005, *ApJ*, 627, 960
 Berger, E., Basri, G., Gizis, J. E., et al. 2008a, *ApJ*, 676, 1307
 Berger, E., Gizis, J. E., Giampapa, M. S., et al. 2008b, *ApJ*, 673, 1080
 Berger, E., Rutledge, R. E., Phan-Bao, N., et al. 2009, *ApJ*, 695, 310
 Berger, E., Basri, G., Fleming, T. A., et al. 2010, *ApJ*, 709, 332
 Bhardwaj, A., & Gladstone, G. R. 2000, *RvGeo*, 38, 295
 Bouvier, J., Matt, S. P., Mohanty, S., et al. 2014, in *Protostars and Planets VI*, ed. H. Beuther, R. S. Klessen, C. P. Dullemond, & T. Henning (Tucson, AZ, USA: University of Arizona Press), 433

- Breuer, D., Labrosse, S., & Spohn, T. 2010, *SSRv*, 152, 449
- Burgasser, A. J., Melis, C., Todd, J., et al. 2015, *AJ*, 150, 180
- Burgasser, A. J., Melis, C., Zauderer, B. A., & Berger, E. 2013, *ApJL*, 762, L3
- Burgasser, A. J., & Putman, M. E. 2005, *ApJ*, 626, 486
- Burningham, B., Hardcastle, M., Nichols, J. D., et al. 2016, *MNRAS*, 463, 2202
- Chabrier, G., & Baraffe, I. 2000, *ARA&A*, 38, 337
- Charbonneau, P. 2014, *ARA&A*, 52, 251
- Cook, B. A., Williams, P. K. G., & Berger, E. 2014, *ApJ*, 785, 10
- de Pater, I. 1981, *JGR*, 86, 3397
- de Pater, I., Butler, B. J., Green, D. A., et al. 2003, *Icarus*, 163, 434
- Doyle, J. G., Antonova, A., Marsh, M. S., et al. 2010, *A&A*, 524, A15
- Drake, J. J., Stern, R. A., Stringfellow, G., et al. 1996, *ApJ*, 469, 828
- Dulk, G. A. 1985, *ARA&A*, 23, 169
- Dungey, J. W. 1961, *Physics Review Letters*, 6, 47
- Dupuy, T. J., Forbrich, J., Rizzuto, A., et al. 2016, *ApJ*, 827, 23
- Ekenbäck, A., Holmström, M., Wurz, P., et al. 2010, *ApJ*, 709, 670
- Fleming, T. A., Giampapa, M. S., & Schmitt, J. H. M. M. 2000, *ApJ*, 553, 372
- Forbrich, J., Dupuy, T. J., Reid, M. J., et al. 2016, *ApJ*, 827, 22
- Gagné, J., Faherty, J. K., Burgasser, A. J., et al. 2017, *ApJL*, 841, 1
- Gastine, T., Morin, J., Duarte, L., et al. 2013, *A&A*, 549, L5
- Gillon, M., Jehin, E., Lederer, S. M., et al. 2016, *Natur*, 533, 221
- Gillon, M., Triaud, A. H. M. J., Demory, B.-O., et al. 2017, *Natur*, 542, 7642
- Gizis, J. E., Burgasser, A. J., Berger, E., et al. 2013, *ApJ*, 779, 172
- Gizis, J. E., Williams, P. K. G., Burgasser, A. J., et al. 2016, *AJ*, 152, 123
- Güdel, M. 2002, *ARA&A*, 40, 217
- Güdel, M., & Benz, A. O. 1993, *ApJL*, 405, L63
- Hallinan, G., Antonova, A., Doyle, J. G., et al. 2006, *ApJ*, 653, 690
- . 2008, *ApJ*, 684, 644
- Hallinan, G., Bourke, S., Lane, C., et al. 2007, *ApJL*, 663, L25
- Hallinan, G., Littlefair, S., Cotter, G., et al. 2015, *Natur*, 523, 568
- Harding, L. K., Hallinan, G., Boyle, R. P., et al. 2013a, *ApJ*, 779, 101
- Harding, L. K., Hallinan, G., Konopacky, Q. M., et al. 2013b, *A&A*, 554, A113
- Jaeger, T. R., Osten, R. A., Lazio, T. J., Kassim, N., & Mutel, R. L. 2011, *AJ*, 142, 189
- Jakosky, B. M., Grebowsky, J. M., Luhmann, J. G., & Brain, D. A. 2015, *GeoRL*, 42, 8791
- Jonas, J. L. 2009, *IEEE Proc.*, 97, 1522
- Kao, M. M., Hallinan, G., Pineda, J. S., et al. 2016, *ApJ*, 818, 24
- Kirkpatrick, J. D., Reid, I. N., Liebert, J., et al. 1999, *ApJ*, 519, 802
- Kirkpatrick, J. D., Gelino, C. R., Cushing, M. C., et al. 2012, *ApJ*, 753, 156
- Kochukhov, O., & Lavail, A. 2017, *ApJL*, 835, L4
- Kochukhov, O., Petit, P., Strassmeier, K. G., et al. 2017, *AN*, 338, 428
- Kuznetsov, A. A., Doyle, J. G., Yu, S., et al. 2012, *ApJ*, 746, 99
- Leto, P., Triglio, C., Oskina, L., et al. 2017, *MNRAS*, 467, 2820
- Liebert, J., Kirkpatrick, J. D., Reid, I. N., & Fisher, M. D. 1999, *ApJ*, 519, 345
- Limber, D. N. 1958, *ApJ*, 127, 363
- Linsky, J. L., Wood, B. E., Brown, A., Giampapa, M. S., & Ambruster, C. 1995, *ApJ*, 499, 670
- Lynch, C., Murphy, T., Ravi, V., et al. 2016, *MNRAS*, 457, 1224
- Lynch, C., Mutel, R. L., & Güdel, M. 2015, *ApJ*, 802, 106
- Lynch, C. R., Lenc, E., Kaplan, D. L., Murphy, T., & Anderson, G. E. 2017, *ApJL*, 835, 30
- Martín, E. L., Delfosse, X., Basri, G., et al. 1999, *AJ*, 118, 2466
- McComas, D. J., & Bagenal, F. 2007, *GeoRL*, 34, L20106
- McLean, M., Berger, E., Irwin, J., Forbrich, J., & Reiners, A. 2011, *ApJ*, 741, 27
- McLean, M., Berger, E., & Reiners, A. 2012, *ApJ*, 746, 23
- Metodieva, Y. T., Kuznetsov, A. A., Antonova, A. E., et al. 2017, *MNRAS*, 465, 1995

- Miles-Páez, P. A., Metchev, S. A., Heinze, A., & Apai, D. 2017, *ApJ*, 840, 83
- Miles-Páez, P. A., Zapatero Osorio, M. R., & Pallé, E. 2015, *A&A*, 580, L12
- Mohanty, S., Basri, G., Shu, F., Allard, F., & Chabrier, G. 2002, *ApJ*, 571, 469
- Morin, J., Donati, J. F., Petit, P., et al. 2010, *MNRAS*, 407, 2269
- Nichols, J. D., Burleigh, M. R., Casewell, S. L., et al. 2012, *ApJ*, 760, 59
- Osten, R. A., Hawley, S. L., Bastian, T. S., & Reid, I. N. 2006, *ApJ*, 637, 518
- Osten, R. A., Melis, C., Stelzer, B., et al. 2015, *ApJL*, 805, L3
- Osten, R. A., Phan-Bao, N., Hawley, S. L., Reid, I. N., & Ojha, R. 2009, *ApJ*, 700, 1750
- Osten, R. A., Brown, A., Ayres, T. R., et al. 2004, *ApJS*, 153, 317
- Paty, C., Paterson, W., & Winglee, R. 2008, *JGR*, 113, A06211
- Perley, R. A., Chandler, C. J., Butler, B. J., & Wrobel, J. M. 2011, *ApJL*, 739, L1
- Phan-Bao, N., Osten, R. A., Lim, L., Martín, E. L., & Ho, P. T. P. 2007, *ApJ*, 658, 553
- Pineda, J. S., Hallinan, G., Kirkpatrick, J. D., et al. 2016, *ApJ*, 826, 73
- Ravi, V., Hallinan, G., Hobbs, G., & Champion, D. J. 2011, *ApJL*, 735, L2
- Reid, I. N., Kirkpatrick, J. D., Gizis, J. E., & Liebert, J. 1999, *ApJL*, 527, L105
- Reiners, A., Schuessler, M., & Passegger, V. M. 2014, *ApJ*, 794, 144
- Robertson, P., Mahadevan, S., Endl, M., & Roy, A. 2014, *Sci*, 345, 440
- Rodríguez, L. F., Zapata, L., & Palau, A. 2017, *AJ*, 153, 209
- Rodríguez-Barrera, M. I., Helling, C., Stark, C. R., & Rice, A. M. 2015, *MNRAS*, 454, 3977
- Route, M., & Wolszczan, A. 2012, *ApJL*, 747, L22
- . 2016, *ApJL*, 821, L21
- Rutledge, R. E., Basri, G., Martín, E. L., & Bildsten, L. 2000, *ApJL*, 538, L141
- Saar, S. H., & Linsky, J. L. 1985, *ApJ*, 299, 47
- Santos-Costa, D., & Bolton, S. J. 2008, *P&SS*, 56, 326
- Sault, R. J., Oosterloo, T., Dulk, G. A., & Leblanc, Y. 1997, *A&A*, 324, 1190
- Schrijver, C. J. 2009, *ApJL*, 699, L148
- Semel, M. 1989, *A&A*, 225, 456
- Shields, A. L., Ballard, S., & Johnson, J. A. 2016, *Phys. Rep.*, 663, 1
- Skumanich, A. 1972, *ApJ*, 171, 565
- Stelzer, B., Micela, G., Flaccomio, E., Neuhäuser, R., & Jayawardhana, R. 2006, *A&A*, 448, 293
- Stelzer, B., Alcalá, J., Biazzo, K., et al. 2012, *A&A*, 537, A94
- Tinney, C. G., & Reid, I. N. 1998, *MNRAS*, 301, 1031
- Treumann, R. 2006, *A&ARv*, 13, 229
- Trigilio, C., Leto, P., Umama, G., Leone, F., & Buemi, C. S. 2004, *A&A*, 418, 593
- West, A. A., Hawley, S. L., Bochanski, J. J., et al. 2008, *AJ*, 135, 785
- White, S. M., Kundu, M. R., & Jackson, P. D. 1989, *A&A*, 225, 112
- Williams, P. K. G., & Berger, E. 2015, *ApJ*, 808, 189
- Williams, P. K. G., Berger, E., Irwin, J., Berta-Thompson, Z. K., & Charbonneau, D. 2015a, *ApJ*, 799, 192
- Williams, P. K. G., Casewell, S. L., Stark, C. R., et al. 2015b, *ApJ*, 815, 64
- Williams, P. K. G., Cook, B. A., & Berger, E. 2014, *ApJ*, 785, 9
- Williams, P. K. G., Gizis, J. E., & Berger, E. 2017, *ApJ*, 834, 117
- Wolszczan, A., & Route, M. 2014, *ApJ*, 788, 23
- Wong, A.-S., Yung, Y. L., & Friedson, A. J. 2003, *GeoRL*, 30, 1447
- Wright, N. J., Drake, J. J., Mamajek, E. E., & Henry, G. W. 2011, *ApJ*, 743, 48
- Wu, C. S., & Lee, L. C. 1979, *ApJ*, 230, 621
- Yantis, W. F., Sullivan, III, W. T., & Erickson, W. C. 1977, *BAAS*, 9, 453
- Yu, S., Doyle, J. G., Kuznetsov, A., et al. 2012, *ApJ*, 752, 60
- Zarka, P., Treumann, R. A., Ryabov, B. P., & Ryabov, V. B. 2001, *Ap&SS*, 277, 293